

11

Pairing in exotic nuclei

Much of the recent research in nuclear structure focuses on nuclei near the neutron and proton drip lines. These are the *loci* in the chart of nuclides of the isotopes and isotones which are stable against neutron and proton emission and which have the largest number of neutrons and protons respectively. The most exotic of these nuclei, which have been produced in the laboratory, are light nuclei lying just within the drip lines. The nucleus ${}^9_3\text{Li}_8$, containing three protons and eight neutrons, is bound by only a few hundred keV and is one of the best-studied examples of a ‘halo’ nucleus to date.

According to the shell model, two of the six neutrons in the ${}^9\text{Li}$ nucleus occupy the lowest $s_{1/2}$ orbital while the remaining four neutrons fill the $p_{3/2}$ orbital. The separation energy of the last neutron in ${}^9\text{Li}$ is $S_n \sim 4$ MeV which is typical for a light nucleus. The halo nucleus ${}^{11}\text{Li}$ has two neutrons outside a ${}^9\text{Li}$ core and the simple shell model predicts that they should fill the $p_{1/2}$ orbital. A special feature of ${}^{11}\text{Li}$ is that the last two neutrons are bound by only 290 keV, while the last neutron in ${}^{10}\text{Li}$ is not bound. A consequence of the small binding energy of the last two neutrons in ${}^{11}\text{Li}$ is that the radius of the orbital they occupy is much larger than the radius of the ${}^9\text{Li}$ core. They form a low-density cloud or ‘halo’ around the core.

In simple versions of the shell model the $s_{1/2}$ level from the s – d shell has an energy which is significantly larger than the $p_{1/2}$ level but in light neutron-rich nuclei the energy difference between these two levels decreases and there is evidence that in ${}^{10}\text{Li}$ the $s_{1/2}$ level lies below the $p_{1/2}$ level. In that case the last two neutrons in ${}^{11}\text{Li}$ might occupy the $s_{1/2}$ level. Consequently, the ${}^{11}\text{Li}$ ground state has a more complicated structure than that predicted by the pure independent particle model, which involves both the $s_{1/2}$ and the $p_{1/2}$ orbitals. The self-energy due to the neutron–phonon interaction is a possible mechanism for the change in the relative energies of the $s_{1/2}$ and $p_{1/2}$ levels.

It is still an open question which mechanisms provide the glue needed to bind the two halo neutrons to the tightly bound ${}^9_3\text{Li}_6$ core. To some extent, this problem seems to be similar to that of the instability of the normal state of an electron system at zero temperature, solved by Cooper, a solution which is at the basis of BCS theory of superconductivity. The main difference with the present case is associated with the shell structure of the system, implying a threshold in the intensity of the attractive interaction needed to produce a bound state (see Chapters 1 and 8). The bare nucleon–nucleon interaction is attractive in the 1S_0 channel and, if it was strong enough, it could bind the last two neutrons in ${}^{11}\text{Li}$. Owing to the fact that the angular momentum content of the space available to the two ‘halo’ neutrons to correlate is low (essentially one s , p and d -orbitals are involved), the system can hardly profit from the large pairing component of the nucleon–nucleon potential (see Section 8.1), as, for example, nucleons in ${}^{120}\text{Sn}$ can (see Figs. 8.4 and 8.9). On the other hand, ${}^{11}\text{Li}$ is highly polarizable displaying a soft dipole mode, as well as collective quadrupole vibrations. As discussed in Chapter 10 there is an induced neutron–neutron interaction due to phonon exchange and there is evidence that the enhancement of the pairing force due to the induced interaction is necessary to bind the ${}^{11}\text{Li}$ nucleus.

Phenomena similar to those mentioned in connection with ${}^{10}_3\text{Li}$ and ${}^{11}_3\text{Li}$ have also been found in the case of ${}^{11}_4\text{Be}$ and ${}^{12}_4\text{Be}$. The main difference with respect to the case of ${}^{11}\text{Li}$ is that both $s_{1/2}$ and $p_{1/2}$ neutron orbitals are bound in ${}^{11}_4\text{Be}_7$, while they are resonant states in ${}^{10}_3\text{Li}_7$. Thus, larger overlaps between the s^2 , p^2 with the d^2 two-neutron configurations are found in ${}^{12}\text{Be}$ compared with ${}^{11}\text{Li}$. The role of the $d_{5/2}$ configuration in the ground state of ${}^{12}\text{Be}$ is consequently quantitatively different than in the case of ${}^{11}\text{Li}$. Furthermore, no soft dipole mode has been observed in ${}^{12}\text{Be}$. Renormalization effects are, in this case, due to quadrupole vibrations.

The focus of this chapter is on the contribution of neutron–phonon coupling to the neutron single-particle energies in ${}^{10}\text{Li}$ and ${}^{11}\text{Be}$ and the binding of ${}^{11}\text{Li}$ and ${}^{12}\text{Be}$. Our discussion is based on results of a study by Barranco *et al.* (2001), Broglia *et al.* (2002) and Gori *et al.* (2004a), results which are to be compared with those of Zukhov (1991, 1993), Esbensen *et al.* (1997), Bertsch and Esbensen (1991), Bertsch (1994) and Sagawa *et al.* (1993).

11.1 The halo nucleus ${}^{11}\text{Li}$

The basic experimental facts which characterize ${}^{11}\text{Li}$ and which are also of particular relevance in connection with pairing in this system are (see Table 11.1): (a) ${}^9_3\text{Li}_6$ and ${}^{11}_3\text{Li}_8$ are stable, ${}^{10}_3\text{Li}_7$ is not; (b) the two-neutron separation energy in ${}^{11}\text{Li}$ is only $S_{2n} = 0.294 \pm 0.03$ MeV (Tanihata (1996)) compared with values of 10 to 30 MeV in normal stable nuclei; (c) ${}^{10}\text{Li}$ displays s - and p -wave resonances

Table 11.1. Single-particle energies associated with the states s and p in ^{10}Li . Two-neutron separation energy S_{2n} , amplitude of the s^2 - and of the p^2 -configurations in the ground-state wavefunctions, mean square radius $\langle r^2 \rangle^{1/2}$ of ^{11}Li and full width $\Delta p_{\perp} = \sigma_{\perp}$ of the momentum distribution of the neutrons emitted in the direction perpendicular to the beam during the breakup of ^{11}Li (after Barranco *et al.* (2001); see also Broglia *et al.* (2002)).

		Theory		
		Exper.	Particle-vibration $+v_{14}$	Mean field
$^{10}\text{Li}_7$ (not bound)	s	0.1–0.2 MeV	0.2 MeV (virtual)	~ 1 MeV (virtual)
	p	0.5–0.6 MeV	0.5 MeV (res.)	-1.2 MeV (bound)
$^{11}\text{Li}_8$ (bound)	S_{2n}	0.294 ± 0.03 MeV	0.330 MeV	2.4 MeV
	s^2, p^2	50%, 50%	40%, 58%	0%, 100%
	$\langle r^2 \rangle^{1/2}$	3.55 ± 0.1 fm	3.75 fm	
	σ_{\perp}	$48 \pm 10 \frac{\text{MeV}}{c}$	$55 \frac{\text{MeV}}{c}$	

at low energy, their centroids lying within the energy range 0.1–0.25 MeV and 0.5–0.6 MeV respectively (Zinser *et al.* (1995)), while these orbitals are well bound in nuclei of the same mass lying along the stability valley; (d) the mean square radius of ^{11}Li , $\langle r^2 \rangle^{1/2} = 3.55 \pm 0.10$ fm (Kobayashi *et al.* (1989), Al-Khalili and Tostevin (1996), Hansen (1996)), is very large compared with the value 2.32 ± 0.02 fm of the ^9Li core, and testifies to the fact that the neutron halo must have a large radius (≈ 6 – 7 fm); (e) the momentum distribution of the halo neutrons is very narrow, its FWHM is $\sigma_{\perp} = 48 \pm 10$ MeV/c for the (perpendicular) distribution observed in the case of the break-up of ^{11}Li on ^{12}C and is of the order of one-fifth of that measured during the break-up of normal nuclei (Kobayashi (1993), Tanihata (1996)); (f) the ground state of ^{11}Li is a mixture of configurations where the two-halo nucleons move around the ^9Li core in s^2 - and p^2 -configurations with almost equal weight (Aoi *et al.* (1997), Simon *et al.* (1999)). The wavefunctions of two-particle-like normal nuclei can be strongly mixed but are, as a rule, dominated by a single two-particle configuration (see e.g. Table 5.1 where the ground-state wavefunctions of ^{210}Pb and ^{206}Pb are given).

Two-neutron halo nuclei are commonly described as three-body systems consisting of two valence neutrons interacting with each other and with a structureless core (see Esbensen *et al.* (1997) and reference therein).

The three-body Hamiltonian can be written as

$$H = \frac{p_1^2}{2m} + \frac{p_2^2}{2m} + V_{nc}(1) + V_{nc}(2) + V_{nn} + \frac{(\vec{p}_1 + \vec{p}_2)^2}{2A_c m}.$$

It includes the kinetic energy of each neutron, their interaction V_{nc} with the core, the interaction between the two valence neutrons, and the recoil kinetic energy of the core, which has the mass number A_c .

The single-particle Hamiltonian for a neutron interacting with the core is

$$h_{nc} = \frac{p^2}{2\mu} + V_{nc}(r),$$

where $\mu = mA_c/(A_c + 1)$ is the reduced mass.

The three-body Hamiltonian then takes the form

$$H = h_{nc}(1) + h_{nc}(2) + V_{nn} + \frac{\vec{p}_1 \cdot \vec{p}_2}{A_c m}. \quad (11.1)$$

This Hamiltonian is to be diagonalized in the space of 0^+ two-neutron states with wavefunctions

$$\Phi_{nn'l_j}(\vec{r}_1, \vec{r}_2) = [\phi_{nl_j}(\vec{r}_1)\phi_{n'l_j}(\vec{r}_2)]_{00},$$

constructed from the eigenstates

$$\phi_{n\ell jm}(\vec{r}) = R_{n\ell}(r) [Y_\ell(\hat{r}) \chi(\sigma)]_{j\ell}$$

of the single-particle Hamiltonian h_{nc} . To do this, one needs to calculate the matrix elements of V_{nn} and of $\vec{p}_1 \cdot \vec{p}_2/A_c m$ between all 0^+ two-particle states. Note that $\vec{p}_1 \cdot \vec{p}_2/A_c m \sim \vec{\nabla}_1 \cdot \vec{\nabla}_2$. Consequently, the matrix elements of the recoil term are intimately connected with the matrix element of the operator (see Appendix in Esbensen *et al.* (1997))

$$\hat{r}_1 \cdot \hat{r}_2 = \sum_m Y_{1m}(\vec{r}_1) Y_{1m}^*(\vec{r}_2).$$

The recoil term, needed to eliminate the spurious centre of mass motion of the system, is intimately connected to an (isoscalar) dipole–dipole field. In fact, the self-consistent value of the dipole–dipole residual interaction needed to describe the giant dipole resonance in the sum-rule conserving RPA leads to a zero-energy isoscalar dipole mode.

A central issue connected with this model is how accurately one must treat the various terms appearing in the Hamiltonian given in equation (11.1).

The ground state of ${}^{11}\text{Li}$ has been studied in several Faddeev and Faddeev-like three-body calculations (Zhukov (1991, 1993)) which make use of a shallow neutron core potential V_{nc} and a simple Gaussian interaction V_{nn} acting between the valence neutrons (see Table 11.2, lines 1 and 2). Calculations with the same V_{nc} but using for V_{nn} a density-dependent (to quench the interaction inside the core)

Table 11.2. Comparison of the ground-state properties of ^{11}Li as calculated by making use of different approaches. Line 5 contains results of nuclear field theory calculations (NFT) discussed in Section 11.1. These results are compared with results published in the literature: (I) obtained with a technique based on a density-dependent, cutoff, contact interaction between the valence neutrons including (lines 3 and 6, Esbensen *et al.* (1997)) and neglecting (lines 4 and 7, Bertsch and Esbensen (1991)) recoil effects, (II) obtained by making use of a Faddeev approach based on realistic interactions (lines 1, 2 (Zhukov (1991), Ian Thompson, *see* Esbensen *et al.* (1997)) and 8 (Zhukov (1993))). The basic quantities that characterize the low-energy nn scattering are the scattering length a_{nn} and the effective range r_{nn} . They are the parameters in the expansion of $k\cot\delta$ in powers of the relative momentum k ($k\cot\delta \approx -1/a_{\text{nn}} + \frac{1}{2}r_{\text{nn}}k^2$), where δ is the s -wave phase-shift. The empirical values are $a_{\text{nn}} = -18.5 \pm 0.5$ fm and $r_{\text{nn}} = 2.8 \pm 0.1$ fm (Bertsch and Esbensen (1991), Zinser *et al.* (1997)).

The results reported in lines 1 and 2 were obtained by making use of a shallow neutron-core potential ($V_{\text{nc}}(r) = -7.8 \exp[-(r/2.55)]$ MeV), which does not support any bound states, and a single Gaussian interaction ($V_{\text{nn}}(r_{12}) = -3(\exp[-(r_{12}/1.8)^2]$ MeV), leading to s -wave phase shifts which are in good agreement with the empirical values. The results quoted in lines 3 and 4 also made use of the shallow neutron-core potential and a density-dependent contact interaction in the $T = 1$, $S = 0$ channel (quenched inside the core). The two-halo neutrons are allowed to move in a radial box of 40 fm with a cutoff of 25 MeV (line 3) and 15 MeV (line 4) respectively. The results in line 6 are based on a stronger core-neutron interaction (potential) in even-parity states producing an s -wave scattering length of $a_{n0} = -5$ fm. The results shown in line 7 were obtained in the non-recoil limit, with a neutron-core $p_{1/2}$ resonance at 800 keV. A particular set of Faddeev results, based on a $p_{1/2}$ resonance at 200 keV and realistic nn-interaction is shown in line 8. In column 3 we display the low-energy nn-scattering length a_{nn} , in column 4 the two neutron separation energy S_{2n} , in column 6 the neutron separation $\langle r_{\text{n,n}}^2 \rangle^{1/2} = \langle \Phi_{\text{g.s.}} | |\vec{r}_1 - \vec{r}_2|^2 | \Phi_{\text{g.s.}} \rangle^{1/2}$, in column 5 the dineutron core distance $\langle r_{\text{c,2n}}^2 \rangle^{1/2} = \langle \Phi_{\text{g.s.}} | (\vec{r}_1 + \vec{r}_2)^2 | \Phi_{\text{g.s.}} \rangle^{1/2}$, while in column 7 we display the mean square radius $\langle r^2 \rangle_A^{1/2} = (\delta \langle r^2 \rangle + \frac{A_c}{A} \langle r^2 \rangle_{A_c})^{1/2}$ where $\delta \langle r^2 \rangle = \frac{1}{A} (\frac{2A_c}{A} \langle r_{\text{c,2n}}^2 \rangle + \frac{1}{2} \langle r_{\text{n,n}}^2 \rangle)$ (Bertsch and Esbensen (1991)). In columns 8 and 9 we display the probability of the two-particle configurations to appear in the ground-state wavefunction.

Line	Comments	a_{nn} (fm)	S_{2n} (keV)	$\langle r_{\text{c,2n}}^2 \rangle^{1/2}$ (fm)	$\langle r_{\text{n,n}}^2 \rangle^{1/2}$ (fm)	$\langle r^2 \rangle_A^{1/2}$ (fm)	$(s_{1/2})^2$ %	$(p_{1/2})^2$ %
1	HMM ^a	-18.5	300	5	7.8	3.59	98.4	
2	Faddeev ^a	-18.5	318	5.3	7.9	3.66	95.1	
3	Esbensen ^a	-15	318	5.2	7.9	3.64	91.1	
4	Bertsch ^a	-15	318	5.0	8.2	3.63	94.4	
5	NFT	-18.5	330	5.1	8.6	3.75	40	58
6	Esbensen ^b	-15	295	5.1	6.8	3.52	23.1	61.0
7	Bertsch ^b	-15	200	4.9	6.2	3.42	6.1	76.9
8	Q9 ^b	-18.5	295	4.6	6.7	3.41		

^a. Table I Esbensen *et al.* (1997).

^b. Table IV Esbensen *et al.* (1997).

contact pairing interaction have also been published (see lines 3 and 4, Table 11.2) (Esbensen *et al.* (1997), Bertsch and Esbensen (1991), Bertsch (1994)). Note that the density-dependent interaction can simulate three-body forces. These forces have been found, in the most refined many-body calculations of light nuclei available in the literature (see e.g. Pudliner (1995)), to play an important role in obtaining the correct binding energy.

In lines 6, 7 and 8 of Table 11.2, the results of contact interactions and realistic force Faddeev calculations are reported, where the parameters of V_{nc} and V_{nn} were adjusted so as to ensure the observed position of the $p_{1/2}$ and $s_{1/2}$ resonances and of the 1S_0 phase shifts.

It is seen that in all cases the observed two-neutron separation energy of ^{11}Li is adequately reproduced. The associated mean square radii are in reasonable agreement among each other. Larger variation among the results of the different calculations is found for the amplitude with which the $s_{1/2}^2(0)$ and $p_{1/2}^2(0)$ two-particle configurations enter the ground state of ^{11}Li . To be able to obtain a sizeable $s_{1/2}^2(0)$ component as required by the experimental findings (Aoi *et al.* (1997), Simon *et al.* (1999)) (see line 6 of Table 11.2) one is forced to use a different V_{nc} interaction for even and for odd single-particle states so as to place both the $p_{1/2}$ and the $s_{1/2}$ resonances at the observed values (Esbensen *et al.* (1997)).

None of the above calculations was concerned with the influence that core polarization effects may have in the properties of the system. In Nuñez *et al.* (1996) the three-body model was extended to include explicitly certain core degrees of freedom and the model was applied to ^{12}Be where sizeable effects were found (see Section 11.2).

While the calculations discussed in this section provide an overall account of the experimental findings, they depend on a number of parameters, in particular those associated with V_{nc} (and determining the position of the resonant single-particle state), parameters which are likely to change from case to case, thus reducing the predictive power of the realistic calculations.

It is likely that much of this ambiguity can be eliminated by properly taking into account the influence of core polarization effects. In other words, by generalizing the models discussed above, in particular that of Bertsch and Esbensen (1991) and Esbensen *et al.* (1997), allowing the two neutrons to feel not only the $\vec{p}_1 \cdot \vec{p}_2 / A_c m$, dipole–dipole like interaction, but also to couple to the vibrations of the core of multipoles different from $L = 1$, vibrations which are also strongly modified by the presence of halo neutrons. This constitutes the essence of the paper of Barranco *et al.* (2001) which we discuss in the next section.

11.1.1 Single-particle states in ^{10}Li : effective mass processes

Nuclear field theory (NFT) provides a systematic description of the nuclear spectrum in terms of the motion of the nucleons, of the collective vibrations of the system and of their interweaving. While (dressed) single-particle states

and collective excitations are directly related to the experimental observations, all the degrees of freedom of the nucleus are already exhausted by the single-particle degrees of freedom. Consequently, overcompleteness and Pauli principle correction processes are essential in the NFT description of the nuclear structure (Bes *et al.* (1976a), (1976b), Bortignon *et al.* (1977)).

This treatment is, to a large extent, equivalent to a full shell model calculation. As in the case of such calculations, the mean-field single-particle levels are used and the coupling to core excitations give rise, through self-energy and Pauli (blocking) effects, to parity inversion (Sagawa *et al.* (1993)) (inversion in the sequence between $s_{1/2}$ and $p_{1/2}$ states (resonances)).

Before discussing the sources of pairing correlations in ^{11}Li , one needs to determine the single-particle resonant spectrum of ^{10}Li . The basis of (bare) single-particle states used is determined by calculating the eigenvalues and eigenfunctions of a nucleon moving in the mean field of the ^9Li core, for which one can use a Saxon–Woods potential (Bohr and Mottelson (1969)), of depth $U_0 = -(51 - 30(N - Z)/A)\text{MeV} = -41\text{ MeV}$. The continuum states of this potential are calculated by solving the problem in a box of radius equal to 40 fm, chosen to make the results stable. Arising mainly from Pauli principle effects (Fock potential, see Section 8.2.1) the k -mass is expected to be dependent on the density of the system. While in nuclei along the stability valley $m_k \approx 0.7 m$, it is expected that in ‘halo’ nuclei $0.8 \lesssim m_k/m \lesssim 1$.

While mean-field theory predicts the orbital $p_{1/2}$ to be lower than the $s_{1/2}$ orbital (see Fig. 11.1, I(a)), experimentally the situation is reversed. Similar parity inversions have been observed in other isotones of $^3\text{Li}_7$, such as $^4\text{Be}_7$ (see Section 11.2). Shell model calculations have indicated that the effect of core excitation, in particular of quadrupole type, plays a central role in this inversion (Sagawa *et al.* (1993), see also Vinh Mau (1995)). Within the framework of Chapters 8 and 9, it is important to study the effect of the coupling of the $p_{1/2}$ and $s_{1/2}$ orbitals of ^{10}Li to quadrupole vibrations of the ^9Li core on the properties of the $1/2^+$ and $1/2^-$ states of this system. Monopole and dipole vibrations have no low-lying strength in this nucleus and their coupling to the single-particle states of ^{10}Li lead to negligible contributions. The quadrupole vibrational state of ^9Li can be calculated by diagonalizing, in the random phase approximation (RPA), a quadrupole–quadrupole separable interaction (see e.g. (8.39)) taking into account the contributions arising from the excitation of particles into the continuum states. A natural choice of the coupling constant is the self-consistent value introduced in equations (8.58) and (10.27). A similar calculation carried out using this value for the neighbouring nucleus, ^{10}Be , yields good agreement with the experimentally known transition probability of the quadrupole low-lying vibrational state (Ajzenberg-Selove (1988, 1990), Raman *et al.* (1987)).

In the calculation of the renormalization effects of the single-particle resonances of ^{10}Li due to the coupling to vibrational states one has to consider not only the effective-mass-like diagrams (upper part graph of Fig. 11.1, I(b))

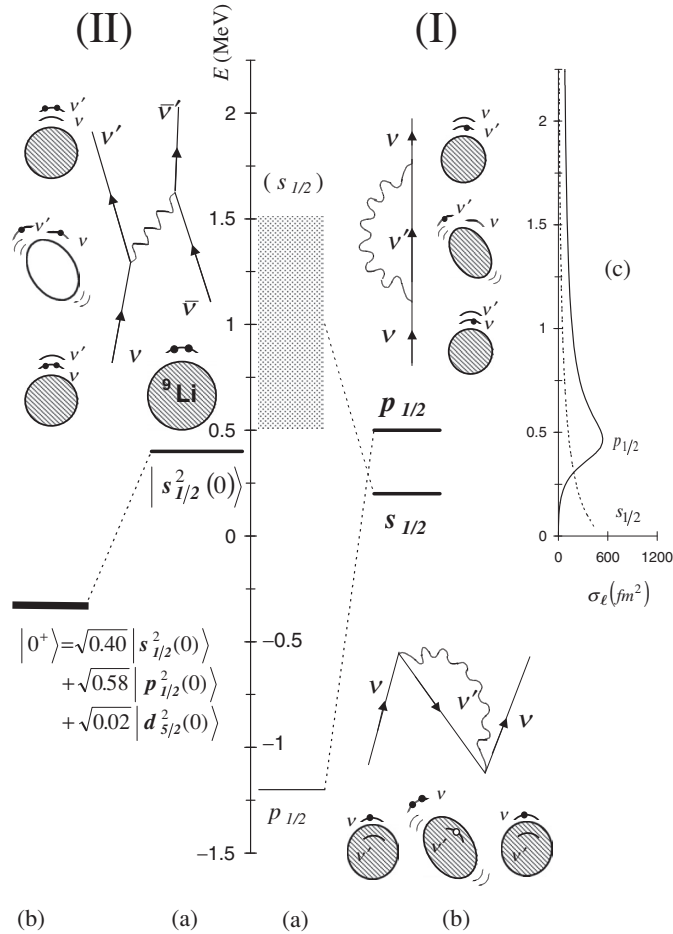


Figure 11.1. (I) Single-particle neutron resonances in ^{10}Li . In (a) the position of the levels $s_{1/2}$ and $p_{1/2}$ calculated using mean-field theory is shown (dotted area and thin horizontal line respectively). The coupling of a single-neutron (upward-pointing arrowed line) to a vibration (wavy line) calculated using the Feynman diagrams shown in (b) (schematically depicted also in terms of either solid dots (neutron) or open circles (neutron hole) moving in a single-particle level around or in the ^9Li core (hatched area)), leads to conspicuous shifts in the energy centroid of the $s_{1/2}$ and $p_{1/2}$ resonances (shown by thick horizontal lines) and eventually to an inversion in their sequence. In (c) we show the calculated partial cross-section σ_ℓ for neutron elastic scattering off ^9Li . (II) The two-neutron system ^{11}Li . We show in (a) the mean-field picture of ^{11}Li , where two neutrons (solid dots) move in time-reversal states around the core ^9Li (hatched area) in the $s_{1/2}$ resonance leading to an unbound $s_{1/2}^2(0)$ state where the two neutrons are coupled to zero angular momentum. The exchange of vibrations between the two neutrons shown in the upper part of the figure leads to a density-dependent interaction which, added to the nucleon–nucleon interaction (v_{14} Argonne), correlates the two-neutron system leading to a bound state $|0^+\rangle$, where the two neutrons move with probability 0.40, 0.58 and 0.02 in the two-particle configurations $s_{1/2}^2(0)$, $p_{1/2}^2(0)$ and $d_{5/2}^2(0)$ respectively (after Barranco *et al.* (2001)).

Table 11.3. RPA wavefunction of the collective low-lying quadrupole vibration of ^9Li (X and Y are the forward-going and backward-going amplitudes respectively, equation (8.38)), calculated using a separable quadrupole–quadrupole interaction (equation (3.50), see also equation (8.44)) and allowing particles to move in the levels of the Saxon–Woods potential discussed in the text. The self-consistent value ($\kappa_2 = 0.013 \text{ MeV}^{-1}$; see equation (8.58)) of the coupling constant has been adopted. The energy of this state is $E_{2^+} = 3.3 \text{ MeV}$. All the listed amplitudes refer to neutron transitions, except for the last two columns. The resulting value for the quadrupole transition probability corresponds to the deformation parameter $\beta_2 = 0.66$. A calculation of the low-lying quadrupole transition in the neighbouring nucleus ^{10}Be with the same coupling constant yields the value $\beta_2 = 0.9$, close to the experimental value $\beta_2 = 1.1$ (Raman *et al.* (1987)).

	$1p_{3/2}^{-1}1p_{1/2}$	$1p_{3/2}^{-1}8f_{7/2}$	$1p_{3/2}^{-1}9f_{7/2}$	$1s_{1/2}^{-1}d_{5/2}$	$1p_{3/2}^{-1}p_{1/2}(\pi)$	$1s_{1/2}^{-1}d_{5/2}(\pi)$
X_{ph}	1.02	0.07	0.08	0.07	0.15	0.09
Y_{ph}	0.28	0.05	0.06	0.06	0.09	0.07

leading to attractive (negative) contributions to the single-particle energies, but also those couplings leading to ground-state correlation (repulsive) corrections associated with diagrams containing two particles, one hole and a vibration in the intermediate states (lower part diagram of Fig. 11.1, I(b) (see Section 9.1, and Fig. 9.2). Because of such ground-state correlation processes, the $p_{1/2}$ state experiences an upward shift in energy. This arises from the coupling of this orbital to the $p_{3/2}$ hole-state through quadrupole vibrational states resulting from the exchange of the odd particle state $p_{1/2}$ with that participating in the vibration, in keeping with the fact that the $(p_{1/2}p_{3/2}^{-1})$ particle–hole excitation constitutes an important component of the quadrupole vibration wavefunction (see Table 11.3). As a consequence, the $p_{1/2}$ state becomes unbound, turning into a low-lying resonance with centroid $E_{\text{res}} \approx 0.5 \text{ MeV}$. Owing to the coupling to the vibrations the s -state is instead shifted downwards. There are essentially no (repulsive) contributions arising from the ground state correlation-correction processes for the s -state.

On the other hand (attractive) effective-mass-like processes with intermediate states consisting of one particle plus a vibrational state of the type $(d_{5/2} \times 2^+)$ lead to a virtual state with $E_{\text{virt}} = 0.2 \text{ MeV}$ (see Fig. 11.1, I(b)). The above results provide an overall account of the s - and p -resonances observed experimentally. The important difference between the distribution of the single-particle strength associated with the resonant state $p_{1/2}$ and the virtual state $s_{1/2}$ can be observed

in Fig. 11.1, I(c), where the partial cross-section σ_l for neutron elastic scattering off ${}^9\text{Li}$ is shown. While σ_p displays a clear peak at 0.5 MeV, σ_s is a smoothly decreasing function of the energy. A small increase in the depth of the potential felt by the s -neutron will lead to a (slightly) bound state, hence the name of virtual resonance.

11.1.2 ${}^{11}\text{Li}$ and the Cooper pair problem

In the infinite system bound Cooper pairs exist for an arbitrarily weak interaction (see Section 1.7), while in the nuclear case this phenomenon occurs only if the strength of the nucleon–nucleon potential is larger than a critical value related to the spacing of single-particle levels in the nuclear spectrum (see Section 1.9). In fact, calculations carried out using v_{14} Argonne NN potential (see Chapter 8) show that the nuclear forces are able to bind Cooper pairs in open-shell nuclei like, for example, ${}^{120}\text{Sn}$ leading to sizeable pairing gaps (see Figs. 8.6 and 8.9), but not in closed-shell nuclei.

The situation is quite different in the case of ${}^{11}\text{Li}$ where the NN-Argonne potential, is not able to bind the last two neutrons. To calculate the spectrum of ${}^{11}\text{Li}$ one places two neutrons in the continuum of levels associated with the $s_{1/2}$ and $p_{1/2}$ resonances as well as in the $d_{5/2}$ states, and diagonalizes the v_{14} NN potential. The calculations show that the bare nucleon–nucleon interaction is not able to bind the two last neutrons to the ${}^9\text{Li}$ core. The low-lying states resulting from the diagonalization of the Argonne nucleon–nucleon force are dominated by one of the configurations $|s_{1/2}^2(0)\rangle$, $|p_{1/2}^2(0)\rangle$ or $|d_{5/2}^2(0)\rangle$. The v_{14} NN potential produces almost no mixing between s -waves, p -waves and d -waves, and only shifts the energy of the unperturbed (resonant) configurations $s_{1/2}^2(0)$ and $p_{1/2}^2(0)$ by about 80 keV without giving rise to a bound system. The $d_{5/2}^2(0)$ configurations are essentially not shifted. Making use of the same single-particle levels and the same matrix elements of the nucleon–nucleon potential to solve the BCS gap equations, one obtains no solution other than the trivial one of zero pairing gap ($\Delta_v = 0$). At the basis of this negative result is the fact that the most important single-particle states which contribute to correlations between the halo neutrons of ${}^{11}\text{Li}$ are the $s_{1/2}$, $p_{1/2}$ and $d_{5/2}$ orbitals. In this low angular momentum phase space, the two neutrons are not able to profit fully from the strong force-pairing interaction associated with the v_{14} NN potential (see equation (8.7)). This is because only the components of multipolarity $L = 0, 1$ and 2 of this force are effective in ${}^{11}\text{Li}$ because of angular momentum and parity conservation rules.

This negative result together with the fact that ${}^{11}\text{Li}$ displays strongly collective, low-lying vibrations suggests that the exchange of these vibrations between the two outer neutrons of ${}^{11}\text{Li}$ is likely to be the main source of pairing correlations in that nucleus (see Fig. 11.2). This effect has been studied by Barranco *et al.* (2001). The $L = 0, 1$ and 2 -vibrational spectrum of ${}^{11}\text{Li}$ needed to calculate the

Table 11.4. RPA wavefunction of the collective low-lying quadrupole phonon in ^{11}Li , of energy $E_{2+} = 5.05$ MeV. All the listed amplitudes refer to neutron transitions, except for the last column. The self-consistent value ($\kappa_2 = 0.013$ MeV $^{-1}$) for the coupling constant was used. The resulting value for the deformation parameter is $\beta_2 = 0.5$.

	$1p_{3/2}^{-1}1p_{1/2}$	$2s_{1/2}^{-1}5d_{3/2}$	$1p_{1/2}^{-1}6p_{3/2}$	$2s_{1/2}^{-1}3d_{5/2}$	$2s_{1/2}^{-1}5d_{5/2}$	$1p_{3/2}^{-1}1p_{1/2} (\pi)$
X_{ph}	0.824	0.404	0.151	0.125	0.126	0.16
Y_{ph}	0.119	0.011	-0.002	-0.049	-0.011	0.07

matrix elements of this induced interaction was determined in much the same way as in ^9Li , i.e. making use of the RPA (see Table 11.3) with the same value of the quadrupole coupling constant. Because the calculations are carried out on the physical (correlated) ^{11}Li ground state, the particle–hole transitions associated with the vibrational states involving the $p_{1/2}$ and the $s_{1/2}$ states are to be calculated with the energies and corresponding occupation numbers resulting from the full diagonalization. The strength of the separable dipole–dipole interaction can be adjusted to provide an overall account of the experimental dipole response in ^{11}Li . Unperturbed particle–hole excitations up to 70 MeV have been included and phonon states up to 50 MeV have been considered. Within this space there are of the order of 10^2 states, exhausting the associated energy-weighted sum rule (Section 8.3). The calculated soft dipole response is shown in Fig. 11.3 (see also Fig. 11.2). The low-lying quadrupole response is concentrated in a single peak, whose wavefunction is shown in Table 11.4. A Skyrme-type effective interaction (SLy4) was instead used to calculate the monopole linear response. The corresponding solutions were obtained in coordinate space making use of a mesh extending up to a radius of 80 fm. The monopole response exhausts 94% of the EWSR considering the summed contributions up to 40 MeV of excitation energy (see Fig. 11.3(c)).

All the resulting vibrational states were coupled to the single-particle states making use of the corresponding transition densities (formfactors, see Fig. 11.3(b) and (d)) and associated particle–vibration coupling strengths. In the monopole case, the response function was discretized in bins of 300 keV.

These calculations, which form the basis of the results shown in Fig. 11.1 and Table 11.1, allowed the two outer neutrons of ^{11}Li both to exchange phonons (induced interaction, Fig. 11.1, II(a)), as well as to emit and later reabsorb them (self-energy correction, Fig. 11.1, I(b)). It was found that the last two neutrons in ^{11}Li form a bound (Cooper) pair, the lowest eigenstate of the associated secular matrix being $E_{\text{gs}} = -0.270$ MeV. This result is mostly due to the exchange of the low-lying dipole vibrations shown in Fig. 11.3(a) with associated wavefunction

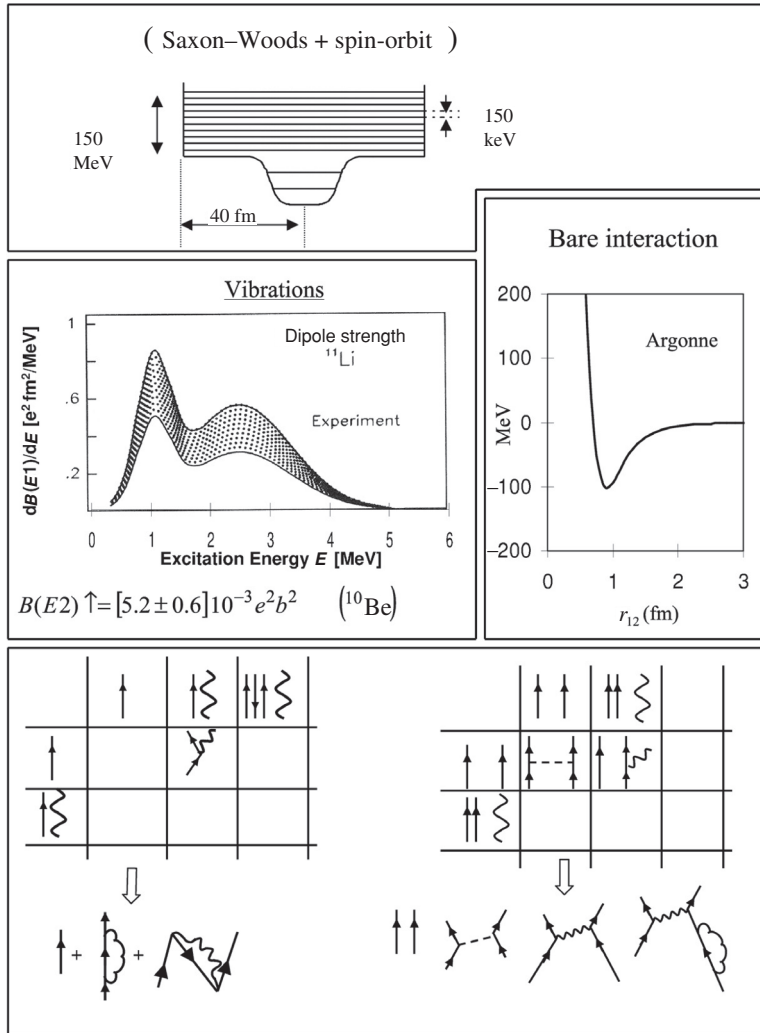


Figure 11.2. In the upper part of the figure, the single-particle potential used to describe the single-particle motion in Li is schematically shown. In the middle left part, the experimental elements used to calculate the strength of the dipole and quadrupole separable interactions are shown, while at the right the dependence of the $T = 1$, $S = 0$ v_{14} Argonne potential on the relative distance r_{12} is displayed. Scattering events up to 200 MeV are to be considered due to the repulsive core of v_{14} . In the lower part of the figure, a schematic representation of the matrices associated with the coupling of neutrons (arrowed lines) through the v_{14} potential (dashed line) and through surface vibrations (wavy lines) for ^{10}Li (left) and ^{11}Li (right) are displayed. The last row shows the basic processes taken into account to all orders in the diagonalization of the corresponding matrices.

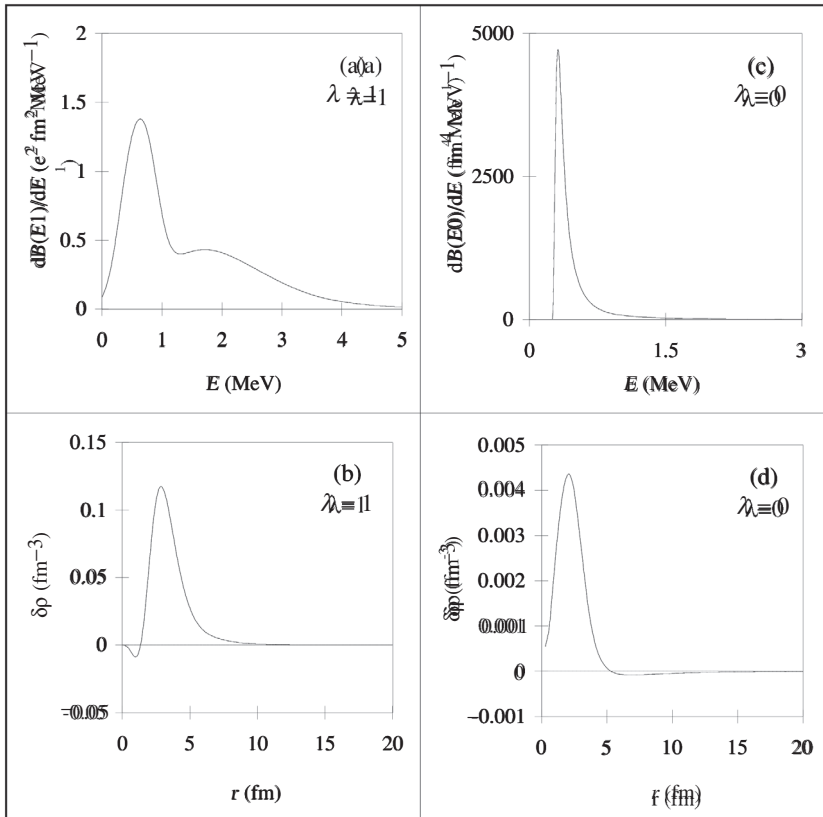


Figure 11.3. Dipole and monopole linear response functions and transition densities of ^{11}Li calculated in the RPA. The dipole response ($\lambda^\pi = 1^-$) was determined making use of the multipole–multipole separable interaction $H = t_c \kappa_1 (F_1(\vec{r}_1) \cdot F_1(\vec{r}_2))_0$, with $F_{1M}(\vec{r}) = r \frac{\partial U}{\partial r} Y_{1M}$. The coupling constant was fixed to provide an overall account of the experimental findings. For simplicity we show in (a) the overall strength function (coarse mesh representation) and not the individual states (about 100). The transition density associated with the state close to the peak, at $E_{1-} = 0.75$ MeV is shown in (b) (see equation (10.47)). The corresponding wavefunction is shown in Table 11.5. No experimental information exists concerning the monopole modes. An effective Skyrme interaction (SLy4) was used to determine the strength function shown in (c). The transition density at the peak ($E_{0+} \approx 0.5$ MeV) is shown in (d) (after Barranco *et al.* (2001)).

collected in Table 11.5. Adding to the induced interaction the nucleon–nucleon v_{14} Argonne potential one obtains $E_{\text{gs}} = -0.330$ MeV, and thus a two-neutron separation energy quite close to the experimental value. Measured from the unperturbed energy of a pair of neutrons in the lowest state calculated for ^{10}Li , namely the s -resonance ($E_{\text{unp}} = 2E_{s_{1/2}} = 400$ keV, see Fig. 11.1, I(b)), it leads to a pairing correlation (Section 3.5) energy $E_0 = E_{\text{unp}} - E_{\text{gs}} = 0.730$ MeV (see Fig. 11.1, II(b)).

Table 11.5. RPA wavefunction of the strongest low-lying dipole vibration of ^{11}Li ($E_{1-} = 0.75$ MeV), contributing most importantly to the pairing induced interaction (Fig. 11.1 II). All the listed amplitudes refer to neutron transitions. The value $\kappa_{1-} = 0.0043$ MeV $^{-1}$ for the isovector coupling constant has been used. It was determined in order to get a good agreement with the experimental findings. Note that this value is quite similar to the self-consistent value of 0.0032 MeV $^{-1}$. The resulting strength function (see Fig. 11.3(a)) integrated up to 4 MeV gives 7% of the Thomas–Reiche–Kuhn energy weighted sum rule (equation (8.51) with $L = 1$), to be compared with the experimental value of 8% (Zinser *et al.* (1997)).

	$1p_{1/2}^{-1}2s_{1/2}$	$1p_{1/2}^{-1}3s_{1/2}$	$1p_{1/2}^{-1}4s_{1/2}$	$1p_{1/2}^{-1}1d_{3/2}$	$1p_{3/2}^{-1}5d_{5/2}$	$1p_{3/2}^{-1}6d_{5/2}$	$1p_{3/2}^{-1}7d_{5/2}$
X_{ph}	0.847	-0.335	0.244	0.165	0.197	0.201	0.157
Y_{ph}	0.088	0.060	0.088	0.008	0.165	0.173	0.138

From the associated two-particle ground-state wavefunction $\Psi_0(\vec{r}_1, \vec{r}_2) (\equiv \langle \vec{r}_1, \vec{r}_2 | 0^+ \rangle)$, Barranco *et al.* (2001) obtain a momentum distribution (whose FWHM is $\sigma_{\perp} = 56$ MeV/c, for ^{11}Li on ^{12}C) and ground-state occupation probabilities of the two-particle states $s_{1/2}^2(0)$, $p_{1/2}^2(0)$ and $d_{5/2}^2(0)$ (0.40, 0.58 and 0.02 respectively, see Fig. 11.1, II(b)), which provide an overall account of the experimental findings. The radius of the associated single-particle distribution is 7.1 fm. Adding to this density that of the core nucleons one obtains the total density of ^{11}Li . The associated mean square radius (3.9 fm) is somewhat larger than the experimental value.

Within the framework of the above discussion it is unlikely that one can obtain a good description of the medium polarization effects in ^{11}Li by coupling the two-halo neutrons to vibrations of ^9Li . In fact, this model gives very different results to those obtained by coupling the vibrations of ^{11}Li to the two-halo neutrons, correcting for Pauli principle violations (Appendix F) (in this connection see Kuo *et al.* (1997)).

Also in this connection, we note that Hamamoto and Mottelson (2003) have studied pairing correlations in weakly bound neutron systems by solving the HFB equations in coordinate space with the correct asymptotic boundary conditions. These are systems where the pair field provides a significant coupling between neutron pairs in the bound state and neutrons moving in the low-energy continuum. Making use of a local pair field of either volume type (that is, $\Delta(r) \sim f(r)$, see equation (8.14) or surface type $\Delta(r) \sim r df(r)/dr$) they found that $s_{1/2}$ neutrons with small binding energies are nearly decoupled from the main pair field. Because $s_{1/2}$ neutrons play a central role in halo nuclei, Hamamoto and Mottelson conclude that the HFB approximation is inadequate to describe these nuclei.

Although the question is quite open, it is likely that this result is another example of the limitations of static mean-field theories discussed at the end of

Section 8.2. These limitations are, at least partially, removed by the dynamic shell model (Mahaux (1985)), taking also into account, in a self-consistent manner, the induced pairing interaction arising from polarization effects.

In fact, the exchange of vibrations with a long tail form factor (see Fig. 11.3(b)) give rise to pairing fields which extend far beyond that associated with the density of the core which is closely connected with the formfactor $f(r)$ (see Barranco *et al.* 2001 as well as Figs. 11.4 and 11.5).

11.1.3 Spatial structure of the Cooper pair

The spatial structure of the Cooper pair described by the wavefunction $\Psi_0(\vec{r}_1, \vec{r}_2)$ is shown in Fig. 11.4. The mean square radius of the centre of mass of the two neutrons is $\langle r_{\text{cm}}^2 \rangle^{1/2} = 5.4$ fm. This result demonstrates the importance that the correlations have in collecting the small (enhanced) amplitudes of the uncorrelated two-particle configuration $s_{1/2}^2(0)$ in the region between 4 and 5 fm, a region in which the $p_{1/2}^2(0)$, helped by the centrifugal barrier, shows a somewhat larger concentration (see Fig. 11.5). From the above results, it emerges that the exchange of vibrations between the least bound neutrons leads to a (density-dependent) pairing interaction acting essentially only outside the core (see also Bertsch and Esbensen (1991)). Note that the long wavelength behaviour of these vibrations is connected with the excitation of the neutron halo, the large size of which not only makes the system easily polarizable but also provides the elastic medium through which the loosely bound neutrons exchange vibrations with each other. Because the vibrational states of ^{11}Li are built out of excitations which occupy, to some extent, the same particle states occupied by the loosely bound neutrons being studied, the corresponding particle-vibration matrix elements have to be corrected because of Pauli violating contributions (see Appendix F) following the nuclear field theory rules (Bes *et al.* (1976a,b), Bes and Broglia (1977), Bortignon *et al.* (1977))). In particular, the reduction factors of the particle-vibration coupling Hamiltonian H_c (see Appendix F) associated with the matrix elements $\langle s_{1/2} \times 1^- | H_c | p_{1/2} \rangle$, $\langle s_{1/2} \times 0^+ | H_c | s_{1/2} \rangle$ and $\langle p_{1/2} \times 0^+ | H_c | p_{1/2} \rangle$ are 0.68, 0.25 and 0.25 respectively.

The average mean square distance between the halo neutrons is $\langle r_{12}^2 \rangle^{1/2} \approx 9.2$ fm, a result which is consistent with the fact that the coherence length associated with Cooper pairs in nuclei is larger than the nuclear dimensions thus preventing the possibility of a nuclear supercurrent. On the other hand, this value of $\langle r_{12}^2 \rangle$ does not prevent the two correlated neutrons being close together, the corresponding (small) probability (see Fig. 11.4) being much larger than that associated with the uncorrelated neutrons (see Fig. 11.5).

Similar results to those reported above are obtained solving the BCS equation for the two-neutron system making use of the matrix elements used in the diagonalization, the sum of those of the nucleon-nucleon v_{14} Argonne

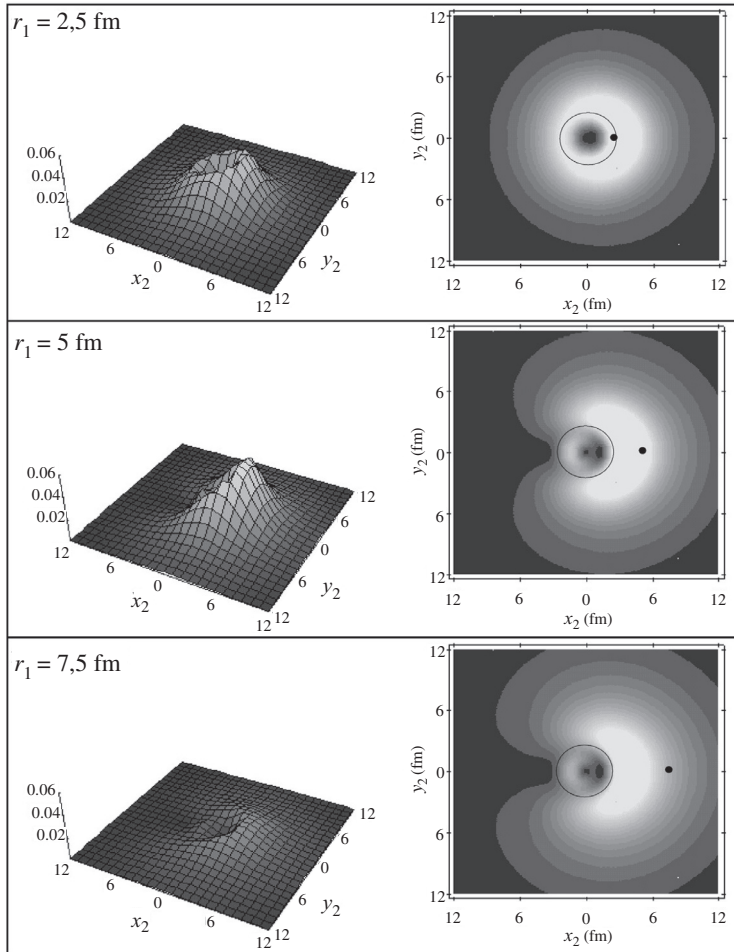


Figure 11.4. Spatial structure of two-neutron Cooper pair. The modulus squared wavefunction $|\Psi_0(\vec{r}_1, \vec{r}_2)|^2 = |\langle \vec{r}_1, \vec{r}_2 | 0^+ \rangle|^2$ (see Fig. 11.1, II (b)) describing the motion of the two-halo neutrons around the ${}^9\text{Li}$ core (normalized to unity and multiplied by $16\pi^2 r_1^2 r_2^2$) is displayed as a function of the cartesian coordinates $x_2 = r_2 \cos(\theta_{12})$ and $y_2 = r_2 \sin(\theta_{12})$ of particle 2, for fixed value of the position of particle 1 ($r_1 = 2.5, 5, 7.5$ fm) represented in the right panels by a solid dot, while the core ${}^9\text{Li}$ is shown as a solid curve circle. The numbers appearing on the z -axis of the three-dimensional plots displayed on the left side of the figure are in units of fm^{-2} (after Barranco *et al.* (2001)).

potential and those of the induced interaction. In this case, the correlation energy is $E_0 = -0.7$ MeV, the separation energy of the two neutrons becoming $S_{2n} = 0.360$ MeV. The radial structure of the projected BCS wavefunctions $\sum_{v>0} (V_v/U_v) \varphi_v(\vec{r}_1) \varphi_v(\vec{r}_2)$ displays a spatial structure quite similar to $\Psi_0(\vec{r}_1, \vec{r}_2)$, the admixture of s -, p - and d -two-particle configurations being now 46%, 51%

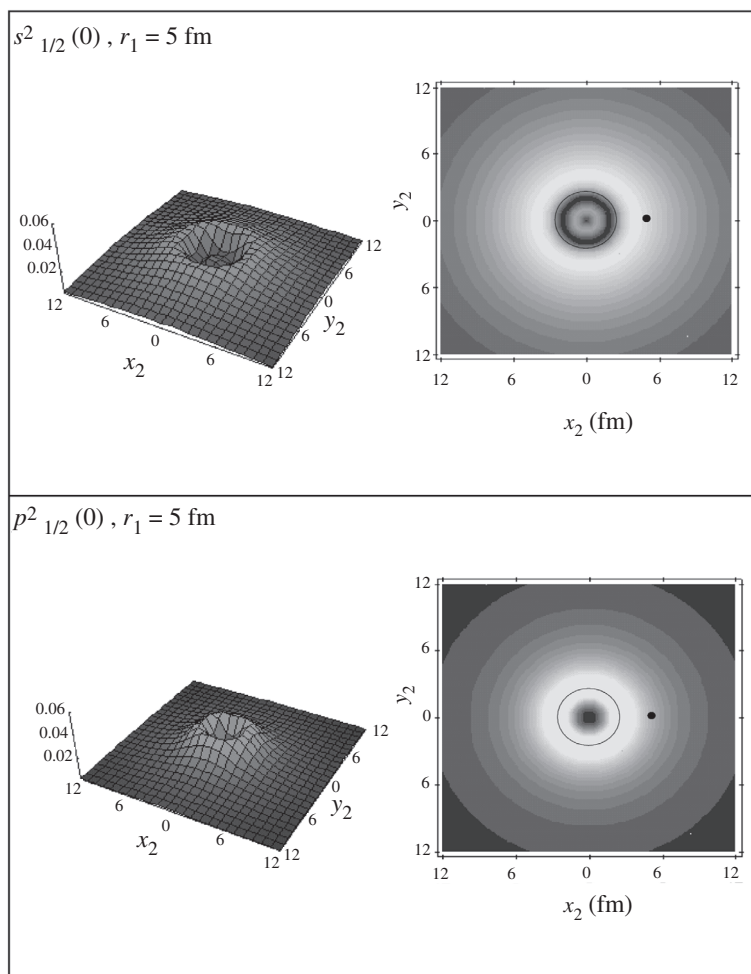


Figure 11.5. Spatial distribution of the pure two-particle configurations $s_{1/2}^2(0)$ and $p_{1/2}^2(0)$ as a function of the x - and y -coordinates of particle 2, for a fixed value of the coordinate of particle 1 ($r_1 = 5 \text{ fm}$). For more details see the caption to Fig. 11.4 (after Barranco *et al.* (2001)).

and 3% respectively. The coherence length ξ , i.e. the mean square distance between the two neutrons forming the Cooper pair, is in this case $\langle r_{12}^2 \rangle^{1/2} = 7.8 \text{ fm}$.

11.1.4 Transfer reactions

The specific probe of pairing correlations is two-particle transfer reactions (see e.g. Broglia *et al.* (1973) and references therein). Combined with single-particle

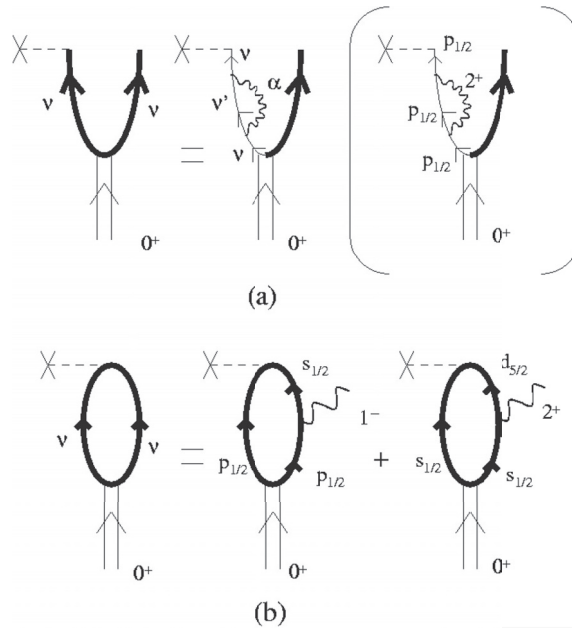


Figure 11.6. (a) Field theoretical representation of the process $^{11}\text{Li}(p, d)^{10}\text{Li}$. A double arrowed line indicates the two-neutron Cooper pair, while a single arrowed heavy drawn curve indicates a nucleon dressed through its coupling to a vibration (wavy line). In parentheses a specific contribution to the dressing process is shown. (b) Field theoretical representation of the two-neutron pick-up process $^{11}\text{Li}(p, t)^9\text{Li}$.

stripping and pick-up reactions (see Fig. 11.6) they can provide a stringent test of the main (microscopic) predictions that nuclear field theory makes concerning ^{10}Li and ^{11}Li , namely

$$|\tilde{s}_{1/2}\rangle = a|s_{1/2}\rangle + b|d_{5/2} \times 2^+; \frac{1}{2}^+\rangle + c|p_{1/2} \times 1^-; \frac{1}{2}^+\rangle + \dots, \quad (11.2)$$

$$|\tilde{p}_{1/2}\rangle = A|p_{1/2}\rangle + B|p_{1/2} \times 2^+; \frac{1}{2}^-\rangle + C|s_{1/2} \times 1^-; \frac{1}{2}^-\rangle + \dots, \quad (11.3)$$

and

$$|0^+\rangle = \alpha|s_{1/2}^2(0)\rangle + \beta|p_{1/2}^2(0)\rangle + \gamma|d_{5/2}^2(0)\rangle + \delta|(s_{1/2}, d_{5/2}) 2^+ \times 2^+; 0\rangle + \gamma|(s_{1/2}, p_{1/2}) 1^- \times 1^-; 0\rangle + \dots \quad (11.4)$$

In what follows we shall discuss the one-particle spectroscopic factors associated with (d, p) and (p, d) reactions and spectroscopic amplitudes associated with (t, p) and (p, t) reactions. The measurement of these quantities could be, in principle, attempted by making use of inverse kinematics techniques.

11.1.5 Spectroscopic factors

Quite generally the $^9\text{Li}(d, p)^{10}\text{Li}$ reaction may provide information on

$$|\langle \tilde{v} | a_v^+ | g s (^9\text{Li}) \rangle|^2 = \begin{cases} a^2 & \nu = s_{1/2}, \\ A^2 & \nu = p_{1/2}, \end{cases} \quad (11.5)$$

and $^{11}\text{Li}(p, d)^{10}\text{Li}$ (see Fig. 11.6 (a)) on

$$|\langle \tilde{v} | a_v | 0^+ \rangle|^2 = \begin{cases} (\alpha a)^2 & \nu = s_{1/2}, \\ (\beta A)^2 & \nu = p_{1/2}. \end{cases} \quad (11.6)$$

11.1.6 B-coefficients

The spectroscopic amplitudes associated with the two-particle process $^{11}\text{Li}(p, t)^9\text{Li}$ is given by (see Fig. 11.6 (b))

$$B_\nu(0^+) = \langle ^9\text{Li}(g s) | [a_\nu a_\nu]_0 | 0^+ \rangle = \begin{cases} \alpha & \nu = s_{1/2}, \\ \beta & \nu = p_{1/2}, \\ \gamma & \nu = d_{5/2}. \end{cases} \quad (11.7)$$

The two-particle transfer cross-section is

$$\sigma(p, t) \sim \left(\sum_\nu B_\nu(0^+) \right)^2 \approx (\alpha + \beta + \gamma)^2. \quad (11.8)$$

11.2 The halo nucleus ^{12}Be

In what follows we shall study the nuclei $^{11}_4\text{Be}_7$ and $^{12}_4\text{Be}_8$, allowing the nucleons to interact through a nucleon–nucleon realistic potential (Argonne v_{14}) taking also into account the coupling between single-particle motion and collective vibrations of the system as was done in the previous section for the case of ^{11}Li and ^{12}Li . Special emphasis will be made, in the present case, on the calculation of the spectroscopic factors of ^{12}Be which, together with the ground-state occupation probabilities of the two-particle configurations s^2 , p^2 and d^2 , provide the most sensitive predictions for a detailed comparison with the experimental findings (Gori *et al.* (2004a)).

We start by considering the system $^{11}_4\text{Be}_7$ described as one neutron moving around the core $^{10}_4\text{Be}_6$, in keeping with the fact that the value of the neutron separation energy in ^{10}Be is 6.813 MeV compared with the value of 0.504 MeV in ^{11}Be . The single-particle levels are determined by solving the Schrödinger equation

$$\left(-\frac{\hbar^2}{2m_k} \nabla_r^2 + U'(r) \right) \phi_j(r) = \epsilon_j \phi_j(r), \quad (11.9)$$

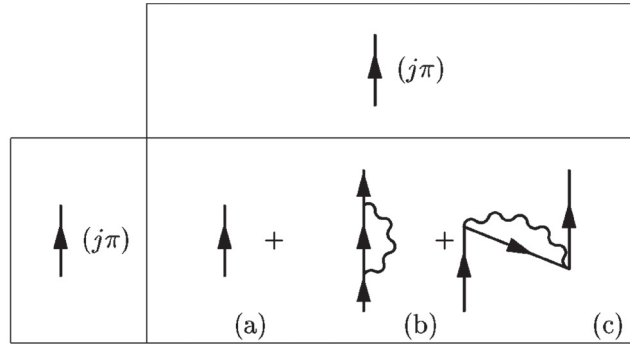


Figure 11.7. Schematic representation of the effective matrix used in the Bloch–Horowitz perturbation theory to calculate the eigenvalues of ^{11}Be (see Section 10.2). An arrowed line pointing upwards (downwards) indicates a particle (hole), while a wavy line indicates a collective vibrational state. Reprinted with permission from Gori *et al.*, *Phys. Rev. C* **69**: 041302 (R) (2004a). Copyright 2004 by the American Physical Society.

in a spherical box of radius equal to 30 fm so as to discretize the continuum states. The quantity m_k is the k -mass while $U'(r) = (m/m_k)U(r)$, $U(r)$ being a Saxon–Woods potential with a standard parametrization for the depth (Bohr and Mottelson (1969))

$$V = -50.5 + 33 \frac{N - Z}{A} \text{ MeV.} \quad (11.10)$$

In keeping with the fact that the k -mass is directly connected with non-locality effects (mainly exchange effects associated with the Fock potential), it is expected to strongly depend on the density of the system. In the case of nuclei along the stability valley, $m_k \approx 0.7m$, while in the case of halo nuclei like ^{11}Be , one expects $0.8m \leq m_k \leq m$. Calculations using both of the limiting values of m_k were carried out, with rather similar results, as explained below.

Making use of the associated particle–hole basis and of a separable multipole–multipole interaction, the $L^\pi = 2^+$ and 3^- vibrations were calculated in the QRPA (equation (8.47)). A self-consistent coupling constant k_L (see equation (10.27)), slightly adjusted to reproduce the energy of quadrupole vibrations, was used. The range of the associated deformation parameters β_L is consistent with observation (Iwasaki *et al.* (2000a,b), Raman *et al.* (1987)).

The eigenvalues of the dressed single-particle states were obtained by diagonalizing (energy-dependent) matrices of the order $10^2 \times 10^2$ whose elements connect a basis of unperturbed states containing both bound and continuum solutions of equation (11.9) with energies up to 350 MeV, with states containing a particle and a vibration (Fig. (11.7(b)) as well as two particles and a hole plus a collective mode (Fig. (11.7(c))). The calculations were carried out for states with quantum number $s_{1/2}$, $p_{1/2}$ and $d_{5/2}$. Similar results were obtained by making use

Table 11.6. Comparison of experimental binding energy and spectroscopic factors with those resulting from the NFT calculations (see Table 11.2, also referred to as particle-vibration $+v_{14}$ (see Table 11.1)) and from an independent particle (mean-field) model. The spectroscopic factors are those for the transfer of one particle on $s_{1/2}$ and $p_{1/2}$ states. They were measured for ^{11}Be and ^{12}Be by Navin *et al.* (2000) and Iwasaki *et al.* (2000a,b) respectively. For ^{12}Be , we also show the components of the resulting ground-state wavefunction (after Gori *et al.* (2004a)).

		Theory		
		Exper.	Particle-vibration	Mean-field
$^{11}\text{Be}_7$	$E_{s_{1/2}}$	-0.504 MeV	-0.48 MeV	~ 0.14 MeV
	$E_{p_{1/2}}$	-0.18 MeV	-0.27 MeV	-3.12 MeV
	$E_{d_{5/2}}$	1.28 MeV(*)	~ 0 MeV	~ 2.4 MeV
	$S [1/2^+]$	0.77	0.87	1
	$S [1/2^-]$	0.96	0.86	1
	$S [5/2^+]$		0.72	1
$^{12}\text{Be}_8$	S_{2n}	-3.673 MeV	-3.58 MeV	-6.24 MeV
	s^2, p^2, d^2		23%, 29%, 48%	0%, 100%, 0%
	$S [1/2^+]$	0.42 ± 0.10	0.31	0
	$S [1/2^-]$	0.37 ± 0.10	0.57	1

* Tentative assignment.

of the unperturbed single-particle basis calculated solving equation (11.9) with $m_k/m = 1$ and $m_k/m = 0.8$, as the larger (absolute) values of the energies ϵ_j are compensated by the stronger particle-vibration coupling vertices proportional to β_L and to $\partial U'/\partial r$ (see equation (8.18)). In what follows we shall refer to the results obtained with $m_k/m = 1$, results which are displayed in Table 11.6, compared with the experimental findings. Theory provides an overall account of the experimental findings, also concerning the spectroscopic factors associated with the reaction $^{10}\text{Be}(d, p)^{11}\text{Be}$ (Zwieglinski *et al.* (1979)). The way these quantities were calculated is discussed below in connection with a shell model calculation carried out in connection with the reaction $^{12}\text{Be}(^9\text{Be}, ^9\text{Be} + n + \gamma)^{11}\text{Be}$ (Navin *et al.* (2000)).

Note that there is experimental evidence of the existence of a resonant $d_{5/2}$ state at 1.28 MeV (Zwieglinski *et al.* (1979), Ajzenberg-Selove (1990)). A calculation was carried out following the steps discussed in Navin *et al.* (2000) but setting the unperturbed energy of the $d_{5/2}$ resonance at 4.1 MeV, so that the dressed resonance had an energy of 1.2 MeV. In this case the spectroscopic factors

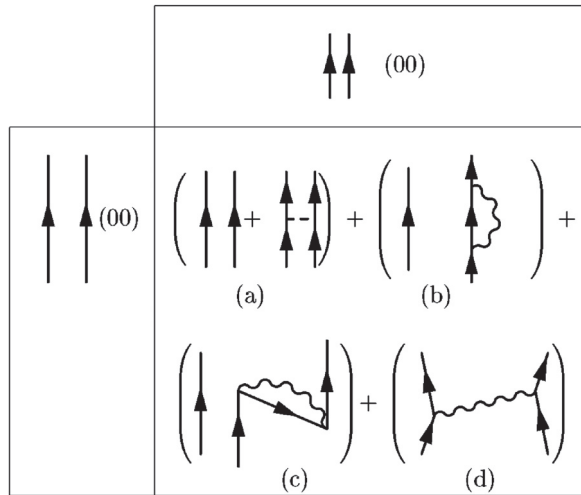


Figure 11.8. Schematic representation of the effective matrix used in the Bloch-Horowitz perturbation theory to calculate the eigenvalues of ^{12}Be . The dashed horizontal line represent the bare (Argonne v_{14}) nucleon–nucleon potential. Pairs of nucleons are coupled to angular momentum $L = 0$. Reprinted with permission from Gori *et al.*, *Phys. Rev. C* **69**: 041302 (R) (2004). Copyright 2004 by the American Physical Society.

associated with ^{11}Be are 0.9, 0.96 and 0.73 respectively, while the ^{12}Be ground-state wavefunction becomes (s^2 , p^2 , d^2) 80%, 5%, 15%.

The self-energy (Fig. 11.7(b)) and Pauli principle correction (Fig. 11.7(c)) processes used to describe the dressed single-particle states of ^{11}Be , which eventually accounted for the parity inversion experimentally observed, have been included in the description of the ground state of ^{12}Be as can be seen from Fig. 11.8, which shows the effective matrix to be diagonalized in order to describe the ground-state properties of the correlated three-body system ^{12}Be (similar calculations carried out by Nuñez *et al.* (1996) did not include processes of type (c), Fig. 11.8). The Hilbert space used to describe ^{12}Be is made out of two-particle states (see Fig. 11.8(a)), two particles and one phonon (Fig. 11.8(b) and Fig. 11.8(d)), and three particles, one hole and one phonon states (Fig. 11.8(c)). All these configurations are coupled to zero angular momentum and display energies up to 500 MeV. The effects of v_{14} and of the particle–vibration coupling in ^{12}Be are determined by diagonalizing the effective, energy-dependent ($\approx 10^3 \times 10^3$) matrix. The lowest eigenvalue -3.58 MeV is to be compared with the experimental two-particle separation energy of -3.67 MeV. The main contribution to the nucleon–nucleon interaction arises from the induced interaction (Fig. 11.8(d)), that associated with the bare nucleon–nucleon potential (see Fig. 11.8(a)) being very small (≈ 100 keV), a situation already encountered in the study of ^{11}Li and associated with the small l -content of the s , p , d -subspace.

The squared amplitudes of the ^{12}Be ground-state wavefunction are shown in Table 11.6. The large $d_{5/2}^2(0)$ -amplitude predicted for the ^{12}Be ground state (see also Navin *et al.* (2000)) compared with that calculated in the case of ^{11}Li can be understood in terms of the fact that the $d_{5/2}$ orbital is, in ^{10}Li , much less confined than in ^{11}Be , thus displaying much smaller overlaps with the $1s_{1/2}$ and $0p_{1/2}$ orbitals. Furthermore, this result is also connected with the fact that in ^{11}Li the dipole mode is much softer than in ^{12}Be (Iwasaki *et al.* (2000a,b)). Using the ^{12}Be ground-state wavefunction and that obtained for the ground state and the first excited state of ^{11}Be , one has calculated the spectroscopic factors associated with the knock-out reaction $^{12}\text{Be} \rightarrow \text{}^9\text{Be}, \text{}^9\text{Be} + n + \gamma \text{}^{11}\text{Be}$. The results are compared in Table 11.6 with the experimental findings (Navin *et al.* (2000)).